Eur. J. Mineral.
2000, **12**, 503-519

Autocorrelation analysis of infrared spectra from minerals

EKHARD K.H. SALJE[1], MICHAEL A. CARPENTER[1], THOMAS MALCHEREK[2] and TIZIANA BOFFA BALLARAN[1]

[1]Department of Earth Sciences, University of Cambridge, Downing Street, Cambridge CB2 3EQ, UK

[2]Centro di Studio per la Cristallografia e la Cristallochimica, via Ferrata 1, I-27100 Pavia, Italy

Abstract: The autocorrelation function, $\mathrm{Corr}(\alpha,\omega') = \int_{-\infty}^{\infty} \alpha(\omega+\omega')\alpha(\omega)\mathrm{d}\omega$, may be used to parameterise effective line widths of absorption bands in IR spectra. It has the advantage of not requiring any peak fitting to the primary spectra and can be applied to individual bands or groups of bands in a spectrum. A new procedure for analysing autocorrelation spectra which result from the application of the autocorrelation function to primary spectra is presented. The approach is well suited for quantifying line width variations in powder absorption spectra from sequences of samples with varying composition, degree of cation order or structural state. Worked examples are set out to illustrate different applications of the approach, including the characterisation of structural phase transitions in tridymite, Al/Si ordering under non-equilibrium conditions in Mg-cordierite, short range Al/Ge order in $BaAl_2Ge_2O_8$ feldspar and mixing behaviour in the jadeite-augite solid solution.

Key-words: IR spectroscopy, autocorrelation analysis, phase transitions, cation ordering, enthalpy variations.

Introduction

Hard mode spectroscopy is a powerful tool for the investigation of phase transitions and chemical mixing phenomena. Any structural change, whether physical, chemical, magnetic, electronic, *etc*., leads to a change of the phonon spectrum. If the structural change is continuous, a general state parameter can be defined which allows these changes to be quantified. In the cases of structural phase transitions or cation ordering, this state parameter becomes the thermodynamic order parameter, Q. As an example, we may envisage Q as the amplitude of a transformation pattern $\Delta\rho$. Let $\rho_i(r)$ be the density function of the initial state (*e.g*., the disordered state) and $\rho_f(r)$ the density function of the final state (*e.g*., the ordered state). Structural evolution may now be described by a pattern function ϕ_i which characterises the structural change, where $\phi \sim (\rho_f(r) - \rho_i(r))$, and an amplitude Q as $\delta\rho(r) = Q\sum\kappa_i\phi_i$. The essence of hard mode spectroscopy is that changes of the phonon spectrum can be treated in perturbation theory with Q as the state variable. In this approximation the three essential parameters of a phonon signal in a Raman or infrared spectrum, namely its integrated intensity I, frequency ω, and line width γ, scale in a simple way with the order parameter as

$$I \sim \omega \sim \gamma \sim AQ + BQ^2 \quad (1)$$

or

$$I \sim \omega \sim \gamma \sim AQ^2 + BQ^4. \quad (2)$$

The first case (Eq. 1) applies only for symmetry changes in which the phonon symmetry is compatible with the symmetry of the order parameter, while the second case (Eq. 2) applies for all other phonon signals (for details see Salje, 1992, 1994,

*email: mc43@esc.cam.ac.uk

DOI: 10.1127/0935-1221/2000/0012-0503 $ 4.25

or Salje & Bismayer, 1997). The parameters A and B can be calculated from model assumptions or from first principles. For many applications, they have been determined experimentally, and it is often found that $A >> B \approx 0$.

In principle, relatively straightforward parameters extracted from a phonon spectrum can give immediate insights into the thermodynamic behaviour of materials undergoing phase transitions. For solids with high symmetry and small unit cells, standard peak fitting procedures are usually used to determine values of I, ω and γ to an adequate degree of precision. Variations of Q with temperature, pressure or composition can then be followed on a comparable basis. Most silicate minerals, however, give complex spectra with multiple overlapping peaks. Even in the best resolved spectra, it may not be possible to decide on the number of modes contributing to an individual group of peaks, let alone produce an objective procedure for fitting them. The primary purpose of this paper is to describe a general method for characterising the band widths in IR spectra from even the most complex of such materials. From the outset it is worth emphasising, first, that the method does not require formal assignment of observed bands to their particular phonon modes, and, second, that it is most effective when small incremental changes between spectra collected at different temperatures and pressures, or with different compositions, are of interest. Other features of phonon spectra, such as LO-TO splitting in spectra from single crystals or weaker changes of the absorption profiles of powder spectra, are irrelevant in this treatment unless the dielectric properties of the material under investigation change substantially during a phase transition. Such effects have been well characterised in ferroelectric and related materials, and equivalent methods for their treatment exist. As far as the present authors are aware for the cases of minerals, no such dielectric anomalies are known which might be detrimental to the perturbation approach used in hard mode spectroscopy. In this paper, weak effects from changes in the LO-TO splitting are not considered, with the understanding that they can easily be included if each of the dispersion parameters is scaled in an appropriate way.

The overall approach makes use of the autocorrelation function and is presented here in four main sections. In the first section, the general background of optical phonon spectroscopy is recalled so as to lead into a mathematical formulation of the proposed methodology. The second section contains a description of the autocorrelation method. A general recipe for its application, based on the autocorrelation spectrum, is then set out in the third section before it is applied to selected mineral examples in the final section. General practitioners of spectroscopy may choose to skip directly to the examples, which are designed to illustrate the procedure for determining variations of line widths in powder absorption spectra from: (a) tridymite, as a demonstration of the effects of displacive transitions, (b) cordierite, as an example of the effects of Al/Si ordering in a more or less continuous sequence of structural states, (c) $BaAlGe_2Si_2O_8$ feldspar, as an example of how local short range order present at equilibrium can be characterised, and (d) Na-rich pyroxenes from the system jadeite - augite, as an example of how mixing behaviour as well as cation ordering may be investigated.

Background

The purpose of this section is to derive the well known spectral functions for IR spectroscopy, but putting emphasis on the fact that damping coefficients have a simple physical meaning and that their investigation can give insights into the nature of phase transitions. The outcome of this treatment is that damping leads to characteristic changes in profile, *e.g.* broadening, and that the damping scales directly with the thermodynamic order parameter. Damping can be treated by perturbation theory, with the obvious result that the temperature/pressure/compositional variation of the damping coefficient is scaled in a simple fashion with the order parameter, independently of the vibrational characteristics (*e.g.* assignment) of a phonon. The starting point is the standard analysis of a damped oscillator (*e.g.* Landau & Lifshitz, 1980); readers familiar with this approach may wish to proceed directly to the next section.

Before we analyse phonon spectra, let us first focus on their origin, namely the time-dependent movement of atomic positions. In the simplest case of a monatomic structure, the equation of motion for one particle is written as a damped oscillator:

$$m\,\ddot{Q}_i = -\,f\,Q_i - m\gamma\dot{Q}_i, \qquad (3)$$

where m is the mass, f is the force constant and γ is a damping parameter. Q_i is the i-th normal coordinate. In the oscillatory regime the time evolution of Q_i becomes, with $\omega_0^2 = f/m$, and $2\gamma < \omega_0$:

$$Q_i(t) = A_i e^{-\frac{\gamma t}{2}}\, e^{i\omega(t-t_0)}. \qquad (4)$$

The frequency ω is given by

$$\omega^2 = \omega_0^2 - \left(\frac{\gamma}{2}\right)^2. \quad (5)$$

More generally, if we consider an atomic position as pushed by any excitation, we can write the time evolution of its movement as

$$m\,\ddot{Q}_i + f\,Q_i + m\gamma\dot{Q}_i = K(t), \quad (6)$$

where K is the force acting on the system. For any arbitrary force, the time response is simply the superposition of the exponential relaxations. More formally, the time evolution is the integral over the Greens function with the kernel of the acting force K. The explicit formula is

$$Q_i(t) = \int_0^\infty \mathrm{d}t'\, \frac{K(t-t')}{m\omega} \mathrm{e}^{-\frac{\gamma t'}{2}} \sin\omega t', \quad (7)$$

with

$$\omega^2 = \omega_0^2 - \left(\frac{\gamma}{2}\right)^2. \quad (8)$$

In the case of an IR absorption experiment, the exciting force is the incident light wave with

$$K = K_0 \cos\Omega t. \quad (9)$$

It is then easy to show that the time evolution of the atomic coordinate is

$$Q(t) = \frac{K_0}{m\omega} \int_0^\infty \mathrm{d}t'\, \mathrm{e}^{-\frac{\gamma t'}{2}} \sin\omega t' \cos\Omega(t-t')$$

$$= \frac{K_0}{m} \frac{(\omega_0^2 - \Omega^2)\cos\Omega t + \gamma\Omega \sin\Omega t}{(\omega_0^2 - \Omega^2)^2 + \gamma^2\Omega^2}. \quad (10)$$

This equation can be understood as forced oscillation with the frequency of the incoming light Ω, a phase angle α and an amplitude Q_0 as

$$Q(t) = \frac{K_0}{m\omega_0^2}\; Q_0 \cos(\Omega t - \alpha) \quad (11)$$

with

$$Q_0 = \frac{\omega_0^2}{\sqrt{(\omega_0^2 - \Omega^2)^2 + \gamma^2\Omega^2}} \quad (12)$$

and

$$\tan\alpha = \frac{\gamma\Omega}{\omega_0^2 - \Omega^2}. \quad (13)$$

The decay of the free oscillator only appears in the damping parameter, which modifies the resonance frequency and the width of the resonance curve. In order to measure γ directly, it would be more convenient to analyse the decay of a phonon signal (as is usually done in pico-second spectroscopy, for example). We show later how the damping can be extracted rather easily from absorption spectra.

We now analyse the same forced oscillation *via* the optical susceptibility and summarise the salient results for the absorption profiles. Using the common notation of optical coordinates (m = 1, $f = \omega_i^2$, $K = -\sqrt{\frac{vf_i}{4\pi}}\,E$, where v is volume) we find the solution of the oscillator equation in the frequency domain directly from Equation 6:

$$Q_i = -\sqrt{\frac{vf_i}{4\pi}} \cdot \frac{E}{\omega_i^2 - \omega^2 + \mathrm{i}\omega\gamma_i}. \quad (14)$$

With the dipole moment

$$P_\alpha = -\frac{1}{\sqrt{4\pi v}} \sum \sqrt{f_i}\; Q_i + \sum \chi_\infty^{\alpha\beta}\; E_\beta, \quad (15)$$

we see that the susceptibility is

$$\chi(\omega) = \frac{1}{4\pi} \sum_i \frac{f_i}{\omega_i^2 - \omega^2 + \mathrm{i}\omega\gamma} + \chi_\infty \quad (16)$$

and the dielectric function is

$$\varepsilon(\omega) = \sum_i \frac{f_i}{\omega_i^2 - \omega^2 + \mathrm{i}\omega\gamma} + \varepsilon_\infty, \quad (17)$$

which can be split into the real part and the imaginary part

$$\varepsilon = \varepsilon' + \mathrm{i}\varepsilon'' \quad (18)$$

with

$$\varepsilon' = n^2 - k^2 = \varepsilon_\infty \sum \frac{(\omega_i^2 - \omega^2)\, f_i}{(\omega_i^2 - \omega^2)^2 + \omega^2\gamma^2} \quad (19)$$

and

$$\varepsilon'' = 2nk = \sum \frac{\omega\gamma\; f_i}{(\omega_i^2 - \omega^2)^2 + \omega^2\gamma^2}. \quad (20)$$

Comparing this result with Equation 11 we see that

$$\varepsilon'' \propto \int_{-\infty}^{\infty} Q_i(0)\, Q_i(t) \mathrm{e}^{\mathrm{i}\omega t} \mathrm{d}t \;=\; \mathrm{FT}(Q_i(0) Q_i(t)).$$

Conversely, the time correlation of $Q_i(t)$ is proportional to the Fourier transform of ε'' : $Q_i(t)Q_i(0) \propto \int_{-\infty}^{\infty} \varepsilon''(\omega)\mathrm{e}^{-\mathrm{i}\omega t}\,\mathrm{d}\omega$. The parameters n and k are the refractive index and the extinction coefficient, respectively. The complex refractive index $N = n + \mathrm{i}k$ is then related to ε *via* $N = \sqrt{\varepsilon}$ and n and k can be easily calculated *via*

$$n = \mathrm{Re}(\sqrt{\varepsilon}) \quad (21)$$

$$k = \mathrm{Im}(\sqrt{\varepsilon}). \quad (22)$$

The optical absorption α is

$$\alpha = 4\pi\omega \mathrm{Im}\sqrt{\varepsilon}. \quad (23)$$

Using the assumption that phonons are well described by damped oscillators, the absorption profile can be calculated directly from

$$\alpha = 4\pi\omega\,\mathrm{Im}(\varepsilon' + \mathrm{i}\varepsilon'')^{½}$$
$$= 4\pi\omega\sqrt{\frac{1}{2}}((\varepsilon'^2 + \mathrm{i}\varepsilon''^2)^{½} - \varepsilon')^{½}, \quad (24)$$

using the expressions for ε' and ε'' in Equations 19 and 20. This line profile of α is highly asymmetric unless the oscillator strength is very small.

In contrast to $\alpha(\omega)$, the optical conductivity $\sigma(\omega)$ is more symmetrical with

$$\sigma(\omega) = \frac{\omega\varepsilon''(\omega)}{4\pi}. \quad (25)$$

Its shape follows directly from $\varepsilon''(\omega)$ in Equation 20.

Measured absorption profiles of powder samples are often even more asymmetric than predicted by Equation 24. No examples are known to the authors where the full theory has been used for quantitative analysis of spectra obtained from minerals. The additional asymmetries are often related to the effective medium effect, which has been explored in great detail in conducting systems such as high temperature superconductors (*e.g.*, Yagil *et al*., 1995). In most insulating minerals the oscillator strengths of the phonon modes are small and the damping γ can be treated as a perturbation parameter. In this case (and only in this case!) we approximate

$$\mathrm{Im}\sqrt{\varepsilon} = \frac{\varepsilon''}{2\sqrt{\varepsilon'}} \quad (26)$$

and $\sqrt{\varepsilon'} = n_\infty$, where n_∞ is the refractive index at high frequencies. In this approximation the absorption coefficient and the theoretically much more elementary optical conductivity have the same line profile, namely that of ε''. This line profile also holds for Raman spectra. The next commonly adopted level of simplification is to reduce the line profile of ε'' for small damping to a Lorentzian shape:

$$\varepsilon''(\omega) = \sum \frac{f_i}{1 + \left(\frac{\omega - \omega_i}{\gamma_i}\right)^2}. \quad (27)$$

This line profile is probably the most commonly used in phonon spectroscopy, although, as shown before, it represents a serious simplification of the theoretically expected profile.

Before the heterogeneous line broadening in phase transitions of the order/disorder type or in chemical mixing is discussed, we summarise the main result so far: the intrinsic absorption profile is asymmetric and can only be approximated by a Lorentzian line profile for small oscillator strength and weak damping. Increasing simplification appears to bury the physically meaningful damping parameter ever deeper in an empirical line profile.

Let us now consider a heterogeneous system. As the characteristic length of hard modes is short on an atomic scale, the macroscopic line profile is the convolution of the intrinsic line profile with the distribution function $\rho(\omega_i)$ of the phonon frequency $\omega_i(r)$:

$$G(\omega) = \int_{-\infty}^{\infty} \rho(\omega - \omega')\alpha(\omega')\mathrm{d}\omega' = \rho \otimes \alpha. \quad (28)$$

In many cases the distribution function $\rho(\omega - \omega')$ is assumed to be Gaussian. With a Lorenztian profile of $\alpha(\omega)$, the resulting macroscopic line profile is the well known (and commonly used) Voigt function, *i.e.*, a mixture of Gaussian and Lorentzian.

The autocorrelation function

It was shown that the phonon spectrum is related, in good approximation, to atomic movements *via* the Fourier transform of the product of the amplitude functions:

$$\varepsilon'' \propto (Q_i^2)_\omega = \mathrm{FT}(Q_i(0)Q_i(t)), \quad (29)$$

where $\varepsilon''(\omega)$ is an even function ($\varepsilon(\omega) = \varepsilon(-\omega)$) defined for ω between $-\infty$ and $+\infty$. This Fourier transform is identical to the product of the Fourier transformed amplitudes

$$Q_i(\omega) = \mathrm{FT}(Q_i(t)) = \frac{1}{2\pi}\int_{-\infty}^{\infty} Q_i(t)\mathrm{e}^{\mathrm{i}\omega t}\mathrm{d}t \quad (30)$$

and the imaginary part of the dielectric susceptibility

$$\varepsilon'' \propto Q_i(\omega)Q_i(-\omega) = Q_i(\omega)Q_i^*(\omega)$$
$$= \int_{-\infty}^{\infty} \phi(t)\,\mathrm{e}^{\mathrm{i}\omega t}\,\mathrm{d}t, \quad (31)$$

where $\phi(t)$ is the autocorrelation function (Press *et al*., 1992):

$$\phi(t) = \int Q_i(t - t')Q_i(t')\mathrm{d}t' = \mathrm{Corr}(Q_i). \quad (32)$$

This close relationship between the absorption profile (or, more precisely, $\varepsilon''(\omega)$) and the phonon amplitude $Q_i(t)$ leads to a simple interpretation of the measured IR spectrum as the Fourier transform of the time autocorrelation function of the phonon amplitudes. As such, it still contains information

on both the homogeneous and heterogeneous line broadening of a band and on the oscillatory movement of the atoms. If we wish to filter out the latter component we need to consider the next higher autocorrelation function. In order to illustrate this argument, let us envisage a Lorentzian line profile

$$(Q_i^2)_\omega = \frac{A}{1+\left(\frac{\omega-\omega_o}{\gamma}\right)^2} \qquad (33)$$

with amplitude A, peak frequency ω_o and line width γ. The time correlation function of the phonon movement is then

$$\phi_i(t) = \mathrm{Corr}(Q_i(t)) = \int_{-\infty}^{\infty} (Q_i^2)_\omega \, e^{-i\omega t} \, d\omega$$

$$= 2\int_0^{\infty} \frac{A}{1+\left(\frac{\omega-\omega_o}{\gamma}\right)^2} e^{-i\omega t} \, d\omega$$

$$= \frac{A}{\gamma} e^{i\omega_o t} \, 2\int_0^{\infty} \frac{1}{1+x^2} e^{-izt\gamma} \, dx$$

$$\propto \pi \frac{A}{\gamma} e^{-i\omega_o t} \; e^{-|t|\gamma}. \qquad (34)$$

The autocorrelation of $\varepsilon''(\omega)$ is then proportional to $\int \phi_i(t) \, \phi_i^*(t) \, e^{+i\omega t} \, dt$, which no longer contains the oscillatory part $e^{i\omega_o t}$. The function

$$\mathrm{Corr}(\varepsilon'') \propto \int_{-\infty}^{\infty} e^{-2\gamma|t|} \, e^{i\omega t} \, dt$$

$$\propto \frac{2\gamma}{\omega^2 + 4\gamma^2} \qquad (35)$$

is again a simple Lorentzian line centred at $\omega_o = 0$. The line width is 2γ, *i.e.*, twice the line width of the peak in the original phonon spectrum. As a result, we find that the autocorrelation of the line profile filters out all the unwanted information about the oscillatory behaviour of the phonons but retains a considerable amount of information about the line profile and, in particular, about the width γ. More complex profiles occur if γ is an explicit function of t, as, for example, in the case of time-dependent random forces interacting with phonons. Such cases are not included in the applications considered here, although an extension of the method to include such effects is straightforward (*e.g.* Petzelt & Dvorjak, 1984).

This procedure can now be generalised for arbitrary line profiles. Any phonon time correlation $\phi(t)$ can be derived by Fourier transformation from $(Q_i^2)_\omega \propto \varepsilon''(\omega)$. It can always be written as an oscillatory function multiplied by some decay function. The former is annihilated by the autocorrelation of $\varepsilon''(\omega)$ which becomes again the Fourier transform of the square of the decay function alone. This means that $\mathrm{Corr}(\varepsilon'')$ contains information about the line profile but no information about the phonon frequency. Thus, $\mathrm{Corr}(\varepsilon'')$ can be used directly for the investigation of the scaling behaviour of γ as desired in Hard Mode spectroscopy and other applications.

Before applications of this analytical method are discussed in detail, three consequences of the theoretical treatment may be expanded upon.

(i) We have seen that the autocorrelation of ε'', $\mathrm{Corr}(\varepsilon'')$, is directly related to the autocorrelation of the phonon amplitude. In other words, $\mathrm{Corr}(\varepsilon'')$ is a higher order autocorrelation of the basic quantity Q_i. We can now consider even higher autocorrelations, *i.e.*, $\mathrm{Corr}^n(\varepsilon'')$ with $n \geq 2$. Such autocorrelations might have advantages for complex line profiles which are the result of the overlap of several phonon signals. While the line profile of the individual phonons is correctly reproduced in $\mathrm{Corr}(\varepsilon'')$ only in the limit $\omega \to 0$, higher order correlations rapidly approach a regular bell-shaped curve with, in general, a Gaussian line profile. A simple rule applies for the line width of each autocorrelation to define the centroid (or "first moment") of a function f as

$$< x > = \frac{\int_{-\infty}^{\infty} x \, f \, dx}{\int_{-\infty}^{\infty} f(x) \, dx} = \frac{i(\mathrm{FT}(f))'_o}{(\mathrm{FT}(f))_o}, \qquad (36)$$

where $(\mathrm{FT}(f))'_o$ means the values of the Fourier transform of $f(\omega)$ for $t \to 0$, *etc.*, for the first derivative. Most autocorrelation functions will have $<x> \approx 0$, even for complex phonon spectra.

The second moment, $<x^2>$, is defined as

$$< x^2 > = \frac{\int_{-\infty}^{\infty} x^2 \, f \, dx}{\int_{-\infty}^{\infty} f \, dx} = -\frac{(\mathrm{FT}(f))''_o}{(\mathrm{FT}(f))_o}. \qquad (37)$$

The variance is then a measure of the line width and is defined as

$$\sigma^2 = <(x - <x>)^2> = \left[\frac{(\mathrm{FT}(f))'_0}{(\mathrm{FT}(f))_0}\right]^2 - \frac{(\mathrm{FT}(f))''_0}{(\mathrm{FT}(f))_0}. \quad (38)$$

The first term will disappear for autocorrelation functions centred at $\omega = 0$. The line width is determined, apart from a normalization factor, by the limit $t \rightarrow 0$ of the second derivative of its Fourier transform. The important lemma is now that, for a = Corr^n (b),

$$\sigma_a^2 = n\sigma_b^2. \quad (39)$$

Thus the variance of any higher order autocorrelation is proportional to the variance of the original spectrum. This important result means that variations of $\sigma_b(Q)$, as measured by Hard Mode spectroscopy, are still reflected in the higher order autocorrelations of the original spectrum.

(ii) Autocorrelations are ideally taken over frequency intervals which contain only one phonon signal. Under most experimental circumstances, phonon spectra of minerals contain a multitude of overlapping peaks. The autocorrelation method can be applied over larger spectral intervals so long as the integration extends over a frequency range which is sufficiently wider than the typical width of any individual phonon signal. The function Corr(ε'') (or Corr(α)) then contains finite size effects in its tails while its centre ($\omega \rightarrow 0$) still reflects truthfully the line profiles of the individual peaks. In the context of this analysis of phase transitions, we envisage the width, γ, of the central part of the autocorrelation function (or its variance) to represent some weighted average of the widths γ_i of the individual peaks. Additional correlations may be contained in γ, although they tend to be small in all examples considered so far. As each γ_i scales in a simple way with the state parameter, γ will then reflect the same scaling. By shifting the frequency interval over which the autocorrelation is calculated, information about the scaling of the individual phonons can be obtained under favourable circumstances. In general, the method is used for the determination of relative changes of the state parameters with, say, temperature, pressure or time. In these cases, the scaling is independent of the spectral range and it is clearly advantageous to choose a frequency interval which shows the largest variation of γ with changing state parameters. An obvious exception to this rule relates to the variation of the characteristic length scale with changing frequency intervals (Salje, 1992, 1994; Salje & Bismayer, 1997; Boffa Ballaran *et al*., 1998a; Atkinson *et al*., 1999).

(iii) It is sometimes convenient to analyse the spectral derivative α' of an absorption spectrum in order to pinpoint the peak frequency, its linewidth, *etc*. A similar procedure is also possible for the autocorrelation function of α. Its first derivative is then related both to α and α' *via*

$$\mathrm{Corr}'(\alpha) = \alpha' \otimes \alpha = \alpha \otimes \alpha' = \int_{-\infty}^{\infty} \alpha'(\omega + \omega')\,\alpha(\omega')\,\mathrm{d}\omega. \quad (40)$$

This function can be used to identify the centroid near $\omega = 0$ and may be useful for filtering high frequency noise in the original spectrum.

The autocorrelation spectrum

The simplest means of demonstrating the procedure used in practice to extract line width information from complex spectra by autocorrelation analysis is to set out a worked example. Fig. 1 contains the merged (Far IR and Mid IR) powder absorption spectra of three different samples of synthetic Mg-cordierite with different

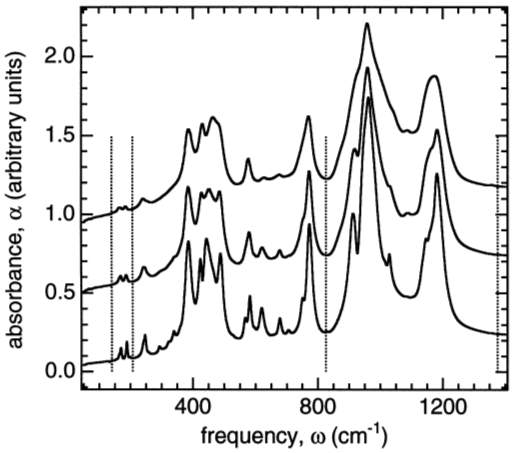

Fig. 1. Merged Far IR and Mid IR spectra of synthetic Mg-cordierite produced by annealing glass of cordierite composition at 1290°C for 2 minutes (top), 77 minutes (middle) and 42 days (bottom). Dotted lines indicate the frequency limits of two segments used for autocorrelation analysis.

states of Al/Si order. The samples were produced by annealing glass of Mg-cordierite composition for 2 minutes (top spectrum), 77 minutes (middle) and 42 days (bottom) in the manner described by Putnis (1980a). A more complete sequence of spectra is given below and similar spectra for the Mid IR range have previously been described by Güttler *et al*. (1989). The autocorrelation analysis of these primary spectra (absorbance, α, against frequency, ω) proceeds as follows.

(i) The primary spectra are separated into segments in such a way that the end points of each segment are on the baseline. The limits of two suitable segments are indicated by dotted lines in Fig. 1, for example, (140 – 208 cm^{-1}, 825 – 1376 cm^{-1}). Segments with single peaks or with groups of peaks may be selected, the critical constraint only being that the limits should be on the baseline. Some suitable baseline between the end points should then be subtracted from each segment; a linear baseline is usually adequate in this context.

(ii) Each segment of the spectrum is correlated with itself, using the autocorrelation function, to produce an autocorrelation spectrum. The autocorrelation function may be written as

$$\mathrm{Corr}(\alpha,\omega') = \int_{-\infty}^{\infty} \alpha(\omega+\omega')\alpha(\omega)\mathrm{d}\omega\,, \quad (41)$$

where $\alpha(\omega)$ is the spectrum itself and $\alpha(\omega + \omega')$ is the same spectrum offset in frequency by ω'. Beyond the limits in ω of the chosen segment of spectrum, $\alpha(\omega) = 0$.

Autocorrelation spectra derived from the 825 – 1376 cm^{-1} segments of IR spectra in Fig. 1 are shown in Fig. 2. The value of Corr for each segment (Corr_{1000} in this case, where the subscript is the value of some wavenumber within the range used for the autocorrelation to serve as a label for that segment) is plotted as a function of offset, ω'. It is immediately clear that the width of the central peak of the autocorrelation spectra varies with the widths of the peaks in the primary spectra. A wide central peak occurs when the primary spectrum has wide absorption bands, and a narrow central peak occurs when the primary spectrum has narrow absorption bands. Sidepeaks arise in the autocorrelation spectrum when adjacent peaks in the primary spectra overlap with increasing ω'.

(iii) Quantitative information on the line widths of a primary spectrum is contained in the width of the central peak of the autocorrelation spectrum, in the limit of $\omega' \to 0$. This can be extracted by extrapolation. A Gaussian curve is fit to the central peak

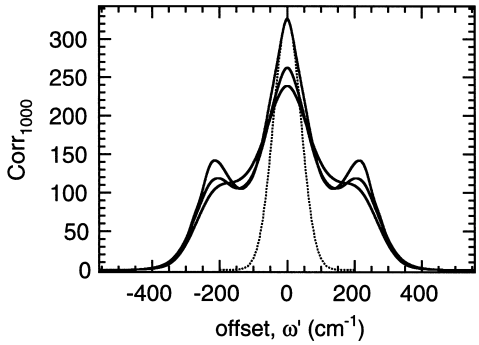

Fig. 2. Autocorrelation spectra from segments of spectra in the range 825 – 1376 cm^{-1} from Fig. 1. The spectrum with the sharpest central peak is from the most ordered sample (42 day anneal) and the spectrum with the broadest central peak is from the least ordered (2 minute anneal). Also shown is a typical Gaussian fit to the central portion of one of the autocorrelation spectra (dotted line).

around $\omega' = 0$ for successive ranges of $\omega' = \pm1, \pm2, \pm3, \ldots$ cm^{-1} (or some other convenient sets of spacings). For this fitting it can be convenient to use a Gaussian function of the form

$$G = k_0 \exp\left[-\left(\frac{x-k_1}{k_2}\right)^2\right]. \quad (42)$$

The coefficient k_2 is related to the width, Γ, of the Gaussian curve by

$$\Gamma = \frac{2.354k_2}{\sqrt{2}}\,. \quad (43)$$

In practice, it may only be variations of the line width which are of interest, and therefore the value of k_2 can be used directly. The value of k_2 from Gaussian fits over different ranges of ω' ($\Delta\omega' = 2$ for $\omega' = -1$ to +1, $\Delta\omega' = 4$ for $\omega' = -2$ to +2, *etc*.) are shown in Fig. 3a for the three autocorrelation spectra in Fig. 2. The value of k_2 at $\omega' = 0$ for the 825 – 1376 cm^{-1} segment, $\Delta\mathrm{corr}_{1000}$, is then obtained by extrapolation, in the present case using a parabolic function. For good quality primary spectra, the value of Δcorr should not be sensitive to $\Delta\omega'$, apart from the influence of adjacent peaks in the primary spectrum starting to overlap with increasing $\Delta\omega'$. For noisy spectra, however, the variations of k_2 at small $\Delta\omega'$ can depend on the noise and not on the true absorption peaks themselves. This is illustrated in Fig. 3b for k_2 derived from the 140 – 208 cm^{-1} segment. The most disordered sample has only weak absorption peaks, and noise in the absorption signal causes k_2 to tail off

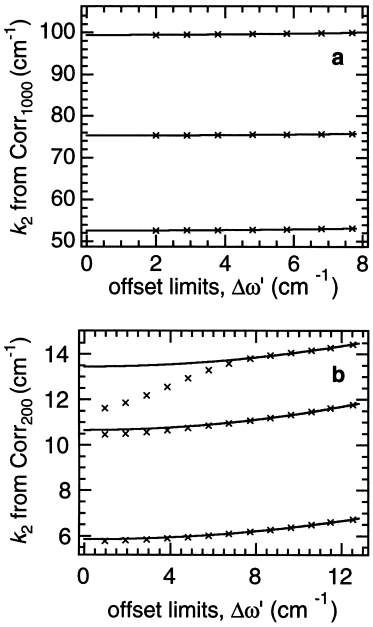

Fig. 3. Variation of k_2 in the Gaussian function (Eq. 42) used to fit the central portion of the autocorrelation spectrum, as a function of the offset range, $\Delta\omega'$, for the fit region. The parameter Δcorr is defined as the value of k_2 at $\Delta\omega' = 0$, and is obtained by extrapolation; a parabolic function has been used here. For k_2 from $Corr_{1000}$, the values of $\Delta corr_{1000}$ are relatively insensitive of the range of $\Delta\omega'$ used, but the values of k_2 at small $\Delta\omega'$ from $Corr_{200}$ are sensitive to noise in the primary spectra.

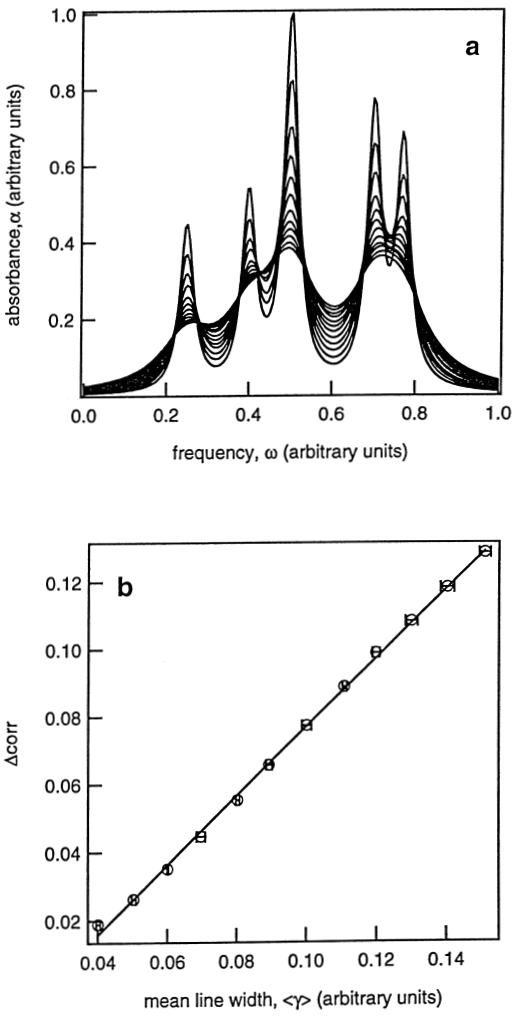

Fig. 4. (a) Synthetic spectra consisting of 5 overlapping peaks with Lorentzian profiles. In each spectrum, the peaks have a different mean width. (b) The variation of Δcorr obtained from the synthetic spectra is linear with the mean line widths of the spectra in (a). The error bars arise from noise added to the synthetic spectra.

as $\omega' \rightarrow 0$. This problem can be circumvented simply by extrapolation from larger $\Delta\omega'$, though it remains desirable to use values of $\Delta\omega'$ which are as small as possible to avoid the influence of peak overlaps in the autocorrelation calculation. Values of Δcorr obtained in this way relate to weighted averages of the line widths of absorption peaks in the chosen segment of primary IR spectrum. The weighting varies with the magnitude of the individual absorption peaks.

An illustration of the possible precision of this method is shown in Fig. 4, using a synthetic spectrum. The synthetic spectrum contains five overlapping peaks, each with a Lorentzian profile and the same width, γ. The value of γ has been adjusted successively to produce the series of spectra shown in Fig. 4a, with some random noise added. Values of Δcorr obtained by autocorrelation analysis of the full sequence of synthetic spectra are plotted against γ in Fig. 4b. As expected, Δcorr is a linear function of mean line width, $<\gamma>$. For a real system, uncertainties propagated from extraction of the values of k_2 and Δcorr are small. Expressed as $\pm 1\sigma$, they are < ~1% for the data shown in Fig. 3, for example. The most significant source of errors is in the preparation of original samples and reproducibility of the primary IR spectra. These cannot easily be quantified, but some indication of their true magnitudes is given by the scatter of extracted values of Δcorr when plotted against other variables such as composition or annealing time.

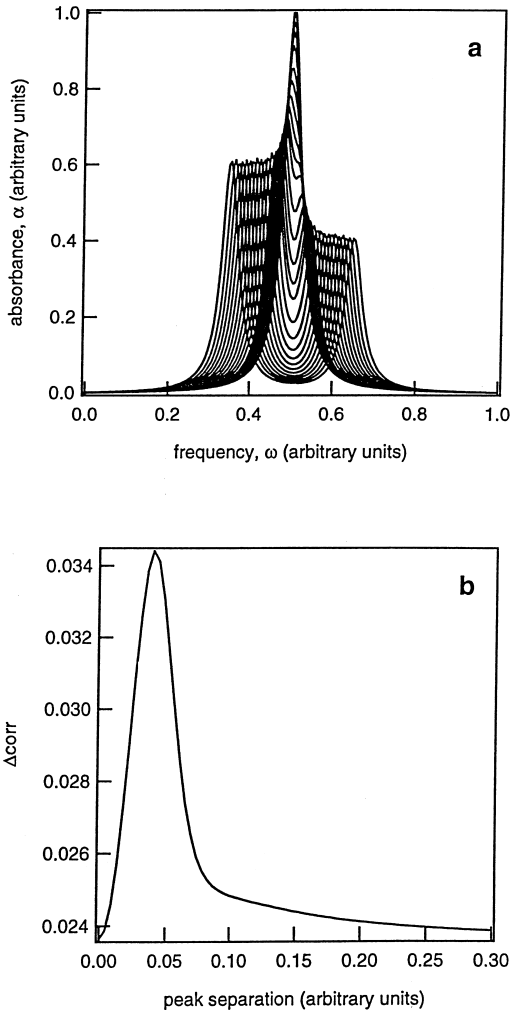

Fig. 5. Synthetic spectra consisting of two overlapping peaks with constant line widths of ~ 0.05 units, but with progressively increasing separation in frequency. (b) Variation of Δcorr as a function of peak separation obtained from the spectra in (a); a more or less constant value of Δcorr is obtained once the peaks have separated by ~ 1.5 times their widths.

Some care is obviously needed in the interpretation of IR spectra from samples which give line width variations that arise more by splitting of absorption bands than by variations of their individual widths. This is illustrated using synthetic spectra in Fig. 5. Two non-equivalent peaks, with some noise, have been set initially to overlap and then progressively to diverge in frequency (Fig. 5a). Autocorrelation analysis of this set of spectra yields the variations of Δcorr shown in Fig. 5b. Each peak has a width at half-height of 0.05 on the scale used, and a realistic measure of this linewidth is not obtained until their centres are separated by ~1.5 times their width (Fig. 5b).

Autocorrelation of the autocorrelation spectrum may be repeated, as discussed in the previous section, but practical applications of multiple autocorrelations have not yet been developed.

Analysis of real systems

In this section, the analysis of IR spectra obtained from a selection of mineral systems is presented. The objective is to illustrate both the methodology and the type of quantitative information which can be obtained from real, *i.e.*, complex, materials. Of interest are the incremental changes that develop when a mineral undergoes a phase transition in response to changing temperature, pressure or composition. It is obviously desirable that noise in the spectral variations due to experimental factors should be minimised. This is achieved by ensuring that: (a) sample preparation methods are as nearly reproducible as possible, (b) data collection parameters are kept constant, and (c) the autocorrelation analysis is repeated over identical ranges, both of ω in the primary spectra and of $\Delta\omega'$ in the autocorrelation spectra. Experience over a number of years has shown that powder absorption spectra from KBr, CsI or polyethylene pellets can be obtained to the required level of reproducibility. In practice this means grinding powder specimens for closely monitored times, weighing both sample and matrix material to a high degree of precision, using a ratio of sample:matrix that is first optimised and then repeated, and, finally, pressing the discs for fixed times under a constant load. In this way internal consistency is maximised. Of much less concern are the absolute values of frequency or line width in the primary IR spectra.

Displacive phase transitions in tridymite

In general, displacive phase transitions give variations in the linewidths of IR spectra which are considerably smaller than the variations associated with cation ordering. If the spectra have multiple overlapping peaks, the chances of extracting quantitative data relating to these variations by conventional peak fitting routines will be small. The sequences of absorption and emission IR spectra

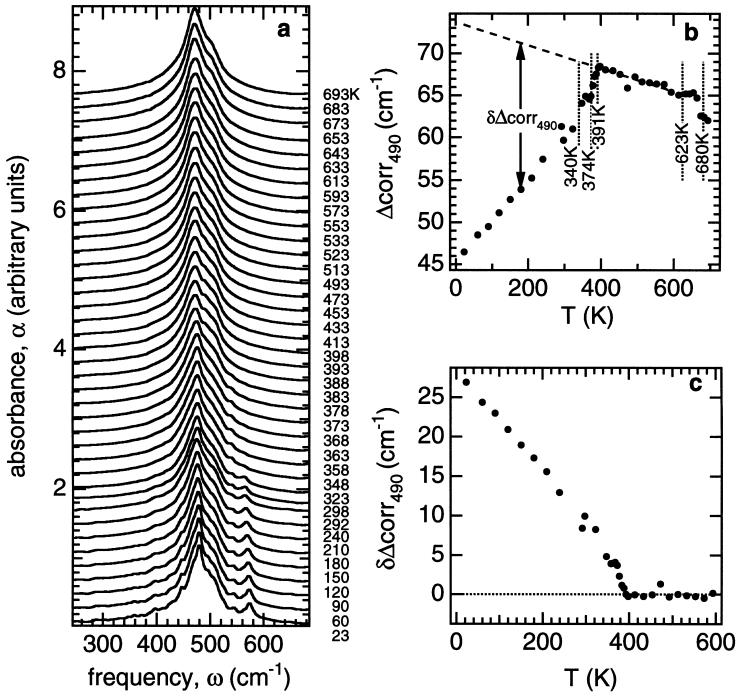

Fig. 6. Autocorrelation analysis of absorption spectra from hand ground meteoritic tridymite. (a) Sequence of segments of spectra collected at temperatures between 23 and 693 K (from Cellai *et al*., 1995). (b) Variations of Δcorr for the spectra in (a); dotted lines indicate known transition temperatures for this material. The major effect is clearly the break in slope at ~ 390 K corresponding to the orthorhombic ↔ monoclinic transition. (c) Variation of the excess line width, δΔcorr, as defined in (b). Two breaks in slope between ~ 340 and 380 K are consistent with there being additional transitions. The break between 292 and 298 K is an artefact arising from a change in experimental data collection techniques.

from meteoritic tridymite shown in Fig. 6a and 7a, respectively, (data from Cellai *et al*., 1995) are typical of just such a displacive system. They are used here to illustrate the effectiveness of the autocorrelation method for determining variations in linewidths.

IR powder absorption spectra of tridymite contain three bands. A set of modes at ~ 350 – 600 cm^{-1} is generally assigned to O-Si-O bending motions, a set at ~ 800 cm^{-1} to Si-O-Si deformation and a set at ~ 1000 – 1300 cm^{-1} to Si-O stretching (Görlich *et al*., 1983; Dowty, 1987; Hofmeister *et al*., 1992). The high temperature hexagonal form gives at least two peaks in each band and the two low temperature forms give many more. Natural and synthetic samples display a variety of phase transitions in the temperature interval 300 – 800 K (most recently reviewed by Xiao *et al*., 1993, 1995; de Dombal & Carpenter, 1993; Withers *et al*., 1994; Cellai *et al*., 1994, 1995; Kitchin *et al*., 1996; Graetsch, 1998), and the IR spectra in this range are expected to be complex. As seen from Fig. 6a, however, any changes that do occur tend to be relatively subtle. Additional peaks appear below ~ 390 K, but changes in the overall width of the ~ 350 – 600 cm^{-1} band are barely visible to inspection.

Values of Δcorr (labelled $\Delta corr_{490}$) obtained by autocorrelation of the spectra in Fig. 6a, following the method described above and using the range 247 – 681 cm^{-1}, are shown in Fig. 6b. Two features of the line width variations represented by $\Delta corr_{490}$ are immediately apparent. First, there is a broad trend of increasing line width from 23 to ~ 395 K, followed by a steady decrease from ~ 395 to 700 K. Second, there are some much smaller anomalies between ~ 395 and 700 K. The cusp at ~ 395 K corresponds to the known position of the orthorhombic ↔ monoclinic transition, which clearly represents the most substantial change that occurs in this temperature interval. In the monoclinic structure, oxygen atoms are essentially

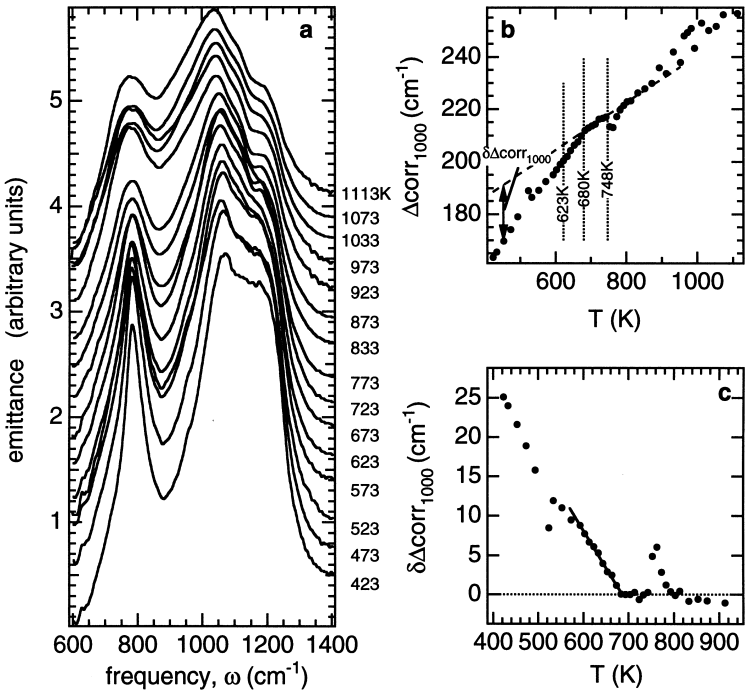

Fig. 7. Emission spectra from meteoritic tridymite. (a) A representative sequence of segments of spectra collected at temperatures between 423 and 1113 K (from Cellai *et al*., 1995). (b) Variation of Δcorr from the emission spectra; dotted lines indicate known transition temperatures. A straight line through the data between 680 and 745 K has been used to define a reference state for the excess line width, δΔcorr. (c) Variation of δΔcorr from (b). The anomaly at ~ 750 K corresponds to a $P6_3/mmc \leftrightarrow P6_322$ transition. There is then a continuous change at ~680 K corresponding to a $P6_322$ (short range order) $\leftrightarrow P6_322$ (long range order) transition which is second order in character. Anomalies at lower temperatures probably correspond to further phase transitions.

ordered, whereas they have substantial positional disorder in the orthorhombic and hexagonal structures (Kihara, 1978; Kihara *et al*., 1986). The changes in positional disorder which occur in the numerous transitions above ~ 395 K produce only minor changes in $\Delta corr_{490}$ and can thus represent only minor structural adjustments.

Taking the data between 400 and 600 K to define a reference state of more or less disorder, an excess linewidth parameter, $\delta\Delta corr_{490}$, can be defined (Fig. 6b). This excess parameter is expected to scale as Q^2 for the orthorhombic $\leftrightarrow$ monoclinic transition and is plotted against temperature in Fig. 6c. The overall transition is known to be split into at least two separate transitions (Cellai *et al*., 1994), and all samples of handground tridymite contain a proportion of the phase MX-1 which transforms to an orthorhombic structure between ~ 310 and 350 K (Hoffmann *et al*., 1983; Xiao *et al*., 1995; Graetsch, 1998). The non-uniform evolution of $\delta\Delta corr_{490}$ just below ~ 395 K reflects these complications and can be followed with a resolution which, from internal consistency, appears to be better than 1 cm^{-1}. A step between 292 and 298 K coincides with the change in instrumental conditions applied during data collection below and above room temperature. It is an artefact which serves to emphasise the need to maintain identical experimental conditions in order to obtain optimal resolution for line width variations.

Details of the higher temperature phase transitions can be detected in the variation of the autocorrelation parameter, $\Delta corr_{1000}$, obtained from the emission spectra shown in Fig. 7a. In this case, the approximately linear variation of $\Delta corr_{1000}$ between 680 and 745 K (Fig. 7b) has been used to define a reference state. The excess parameter $\delta\Delta corr_{1000}$, with respect to this reference state, is shown in Fig. 7c. A distinct anomaly at ~ 750 K coincides with a transition between the $P6_3/mmc$ structure and a $P6_322$ structure with (dynamical or static) disorder, as proposed by de Dombal &

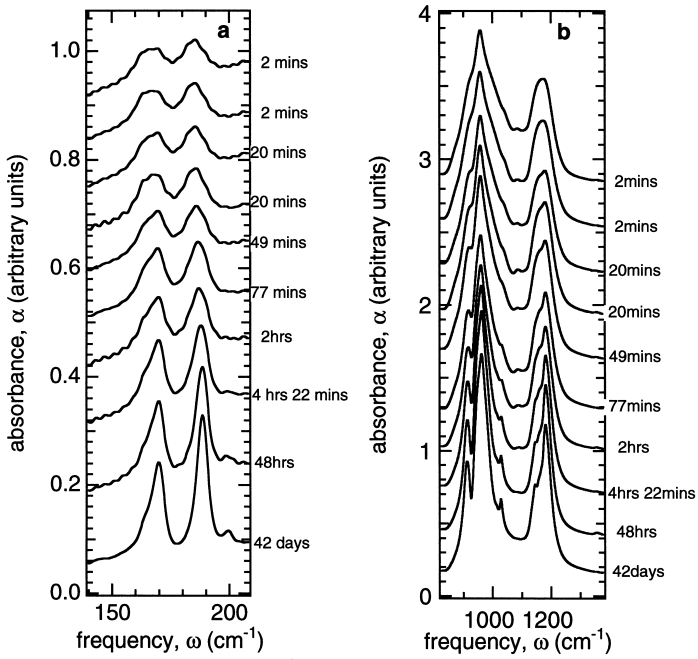

Fig. 8. Segments of IR spectra from a sequence of synthetic Mg-cordierite samples prepared by annealing glass of Mg-cordierite composition for different lengths of time at 1290°C.

Carpenter (1993). The break in slope between 670 and 680 K coincides with a proposed transition between short range ordered and long range ordered states of the $P6_322$ structure (Cellai *et al*., 1994, 1995), and the linear variation of $\delta\Delta corr_{1000}$ between ~ 600 and 680 K is consistent with $Q^2 \propto T$ (second order character). Below ~ 600 K, there are further changes in slope which may correspond to phase transitions in the orthorhombic structure, but there are insufficient data to resolve these clearly. As is found with heat capacity (de Dombal & Carpenter, 1993), there appears to be no obvious anomaly associated with the hexagonal ↔ orthorhombic transition at ~ 625 K. This transition evidently involves a very minor perturbation of the local structure, although it represents a significant break in correlation behaviour over the longer length scale characteristic of X-ray diffraction. Above ~ 900 K the data show substantial scatter (Fig. 7b), presumably from instrumental effects, but, even from apparently the most unpromising of primary spectra, the internal consistency of the data below ~ 900 K suggests that a resolution of better than 1 cm^{-1} is obtainable for the variations in linewidth using autocorrelation analysis.

Al/Si ordering in cordierite

Two segments of spectra from a more complete series of synthetic magnesian cordierite samples crystallised at 1290°C are shown in Fig. 8. The annealing times of between 2 minutes and 42 days generated structural states varying from hexagonal (Al/Si disordered) through modulated to orthorhombic (Al/Si ordered), as described in detail by Putnis (1980a and b) and Putnis & Bish (1983). Structural evolution in this sequence has also been reviewed more recently by Daniels *et al*. (1994). Güttler *et al*. (1989) examined Mid IR spectra from a similar series of samples. They concluded, from the additional peaks that appear in the spectra when the symmetry is lowered, that the modulated structure is in fact locally ordered on the same basis as the orthorhombic structure. By conventional fitting of a group of peaks in the frequency range 550 – 630 cm^{-1}, they also concluded that there is a small discontinuity in the degree of local order when the modulated phase develops at the expense of the hexagonal phase (see, also, Redfern *et al*., 1989). Autocorrelation analysis of the spectra, without the need to fit individual peaks, reveals more detailed insights into the

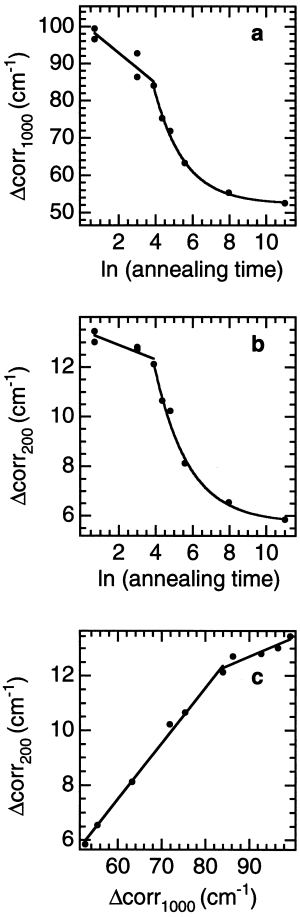

Fig. 9. (a,b) Variations as a function of the logarithm of annealing time for Δcorr derived from the spectra in Fig. 8. Lines and curves are drawn in as guides to the eye. The hexagonal → modulated transition occurs at shorter times than the break in slope. (c) Variations of Δcorr from different frequency ranges of the primary IR spectra: $\Delta corr_{200}$ from spectra in Fig. 8a, $\Delta corr_{1000}$ from spectra in Fig. 8b.

structural evolution. The range between 825 and 1376 cm^{-1} contains many peaks, corresponding, probably, to stretching and bending modes of the tetrahedral framework. The second range chosen, between 140 and 208 cm^{-1}, involves a smaller number of modes. Motions of Mg are probably more important in these. The results of autocorrelation analysis of these two segments are shown in Fig. 9.

The variation of Δcorr with annealing time reflects the variation of the average line widths of peaks in the two spectral ranges and is expected, as a first approximation, to scale with q_{od}^2, where q_{od} is some local order parameter for Al/Si ordering. As shown in Fig. 9a and b, there is a break in slope of the time dependence of Δcorr from both spectral ranges (labelled $\Delta corr_{200}$ and $\Delta corr_{1000}$). This is in marked contrast with NMR determinations which show a linear decrease in the number of Al-O-Al linkages with the logarithm of annealing time through the complete hexagonal → orthorhombic sequence (Putnis & Angel, 1985; Putnis *et al*., 1987). At short annealing times Δcorr for the low frequency range shows a smaller variation than Δcorr for the high frequency range, and the difference is clear in a plot of one against the other (Fig. 9c). The hexagonal → modulated transition occurs after a shorter annealing time than does the break in slope shown in Fig. 9.

The implications of these results for the complete picture of Al/Si ordering in cordierite will be presented elsewhere. For present purposes it is sufficient to make two points. First, if there is a discontinuity between the hexagonal and modulated phase it must be small (see Fig. 9a or b). The abrupt increase in intensity of the mode near 568 cm^{-1}, which Güttler *et al*. (1989) used to infer the existence of a discontinuity, is probably an artefact arising from the uncertainties inherent in fitting a small peak on the flank of a much larger one. Second, Δcorr variations in spectra from modulated and orthorhombic samples vary linearly with each other over the two spectral ranges (Fig. 9c). This is consistent with the expectation that each will vary linearly with q_{od}^2. The high frequency range appears to be more sensitive to local structural changes within the hexagonal and earliest modulated phases in comparison with the low frequency range. This could arise from the different correlation length scales for phonons as a function of frequency. The characteristic length scale of phonons scales with $1/\omega$ (Salje, 1992), and IR modes will "see" the ordering transition at different stages therefore. In particular, if there is a continuous increase in the local degree of Al/Si order with annealing time, this will be reflected in a more or less continuous change in the widths of high frequency modes. The low frequency modes should show marked variations only after the domains of coherent (locally orthorhombic) Al/Si order have exceeded some dimension, perhaps on the order of ~ 10 unit cells.

Al/Ge ordering in $BaAl_2Ge_2O_8$ feldspar

A rather similar picture to the ordering in cordierite emerges from autocorrelation analysis

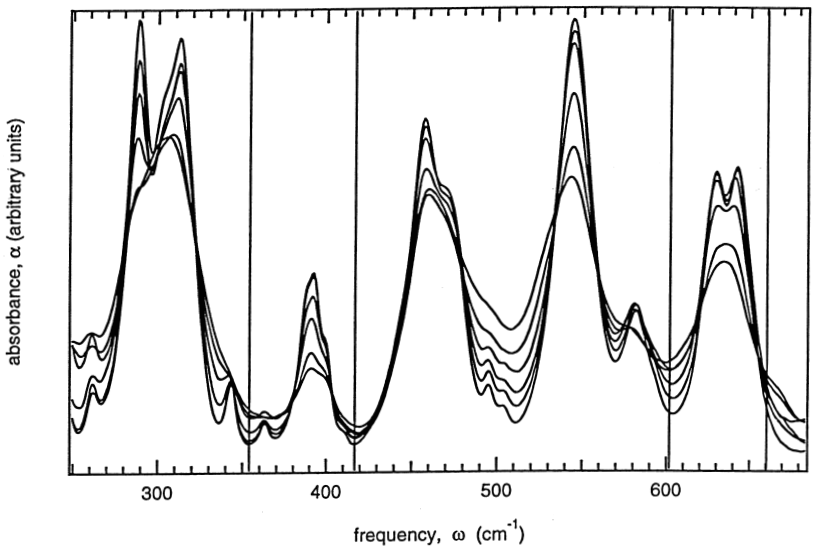

Fig. 10. IR powder absorption spectra obtained from samples of $BaAl_2Ge_2O_8$ feldspar quenched from equilibration temperatures of between 1173 and 1723 K (data from Malcherek *et al*. 1999). Vertical lines indicate the frequency limits of segments analysed using the autocorrelation function.

of powder absorption IR spectra from $BaAl_2Ge_2O_8$, though in this case reflecting changes in the equilibrium degree of order. There is a phase transition $C2/m \leftrightarrow I2/c$ associated with Al/Ge ordering which has an equilibrium transition temperature of ~1690 K (Malcherek *et al*., 1995, 1999). A representative set of IR spectra obtained from samples equilibrated at a range of high temperatures and then quenched are shown in Fig. 10 (from Malcherek *et al*., 1999). Values for Δcorr were determined for two segments of the primary spectra in the ranges 354 – 417 cm^{-1} and 600 – 660 cm^{-1}. (Note that Malcherek *et al*. (1999), in their analysis of these spectra, used an earlier and less refined method for extracting line width information from the autocorrelation spectrum). Because structural data in the form of mean tetrahedral site occupancies of X-ray refinements are also available for these samples, it is possible to test the expected relationships between the IR linewidths, as expressed by Δcorr, and the macroscopic order parameter, Q_{od}. It is expected that Δcorr will vary

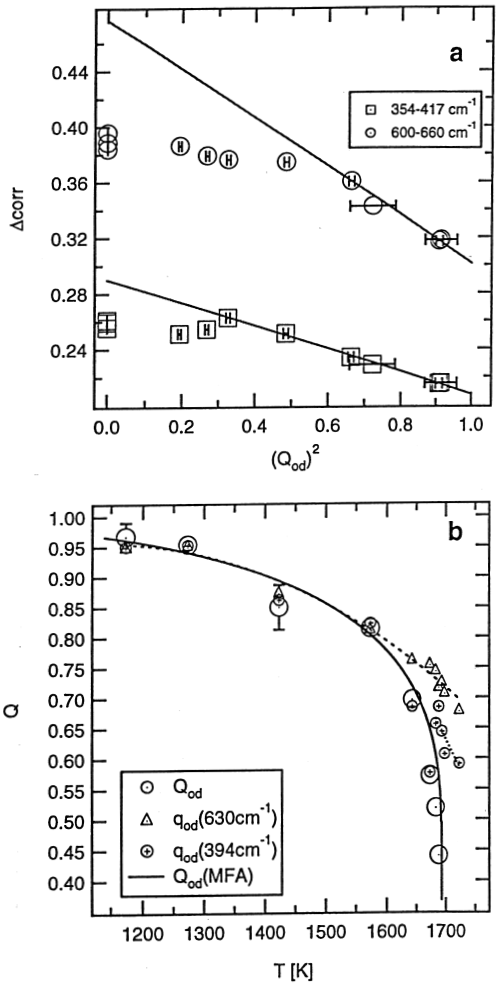

Fig. 11. Variation of Δcorr from two frequency ranges of the primary spectra in Fig. 10 as functions of Q^2_{od} from structure refinements (a) and equilibration temperature (b). The difference in behaviour between Δcorr values from the two frequency ranges might imply local ordering effects on different length scales. Note that the solid line for Q_{od} (MFA) in (b) is the equilibrium variation calculated using a mean field approximation.

with q_{od}^2, where q_{od} is the local order parameter; the average X-ray order parameter, Q_{od}, need not vary linearly with q_{od} if there is any significant short range order in a crystal. The results shown in Fig. 11a can be understood as implying that deviations from $q_{od} \propto Q_{od}$ occur at small values of Q_{od}, and that data from the higher frequency range are more nearly linear than data from the lower frequency range. Again, the scaling of coherence length with $1/\omega$ suggests the discrepancies could be due to short range Al/Ge order on a unit cell length scale which is different from the macroscopic average. The extent of this possible short range order is shown in Fig. 11b; it is closely associated with the transition point and extends into the equilibrium stability field of the *C*2/*m* structure.

Mixing and ordering in the jadeite-augite solid solution

Local structural heterogeneities arise in most materials in association with phase transitions. Hard mode spectroscopy is well developed in this context as a method for characterising the nature and temperature, or time dependence, of such heterogeneities. It is also well known that vibrational spectra can show substantial line broadening as cations are substituted across a solid solution. The line broadening is due to the local heterogeneity of a structure which relaxes differently around cations with different sizes or charges, but is generally treated only qualitatively. Selected results from a study of natural jadeite-omphacite-augite pyroxenes are treated here to illustrate how the approach developed to investigate displacive and

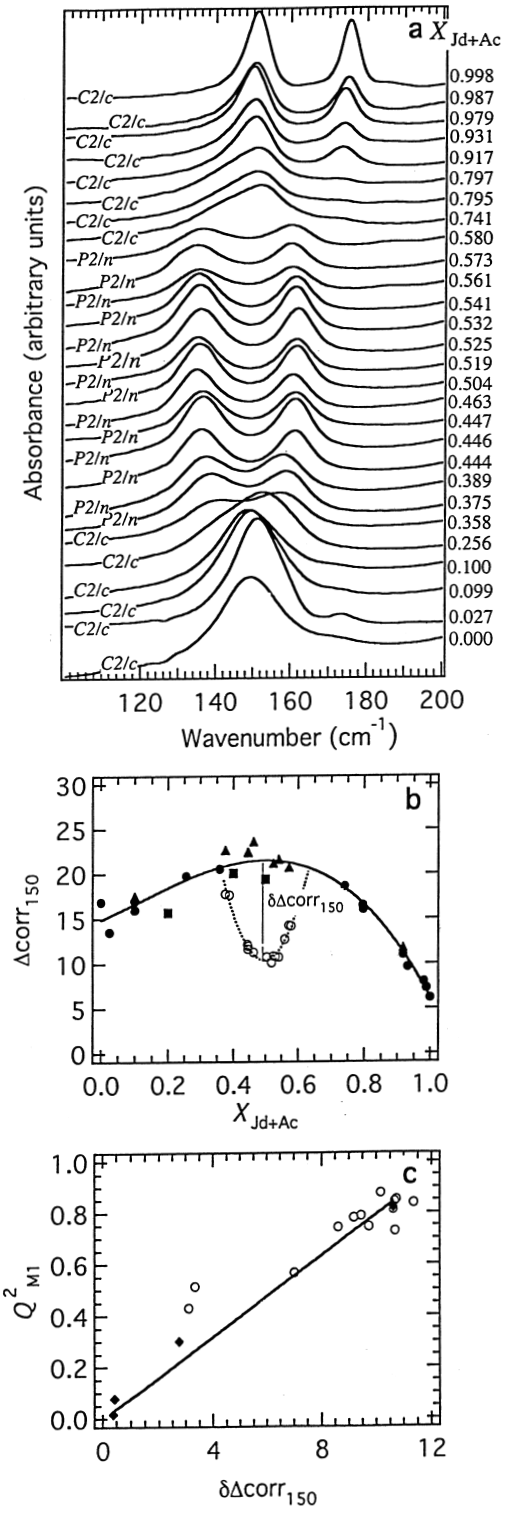

Fig. 12. (a) Representative set of segments of powder absorption spectra from natural samples of pyroxenes belonging to the jadeite-augite solid solution. (Data from Boffa Ballaran *et al*., 1998a). (b) Autocorrelation analysis yields a variation of line width, expressed as $\Delta corr_{150}$, which displays an asymmetric positive excess for the *C*2/*c* (disordered, filled symbols) solid solution and a displacement, $\delta\Delta corr_{150}$, corresponding to cation ordering in the *P*2/*n* structure (open symbols). Composition across the solid solution is expressed in terms of the mole fraction of jadeite + acmite components, X_{Jd+Ac}. (c) The excess line width parameter, $\delta\Delta corr_{150}$, varies linearly with Q^2_{M1}, where Q_{M1} represents the degree of cation order on M1 sites extracted from structure refinements (Boffa Ballaran *et al*., 1998a and b). Open circles represent different ordered samples. Filled diamonds indicate different structural states of a natural sample heat treated for different times at 950°C.

cation ordering transitions can be adapted to investigate the mixing behaviour of solid solutions. A more complete description of this system is given in Boffa Ballaran *et al*. (1998a and b), and references therein. (Note that Boffa Ballaran *et al*. (1998a) also used an earlier, less refined method for extracting Δcorr values from the autocorrelation spectra).

Complete powder absorption IR spectra from a set of natural samples are given in Boffa Ballaran *et al*. (1998a). The 100 – 200 cm^{-1} segment is reproduced in Fig. 12a and was used to determine Δcorr (labelled $\Delta corr_{150}$) values following the recipe given above. At intermediate compositions the natural samples have ordered cations and *P*2/*n* symmetry. Heat treatment of these induces cation disorder and a change to *C*2/*c* symmetry, so that $\Delta corr_{150}$ variations with changing composition and degree of order can be obtained. The variation of $\Delta corr_{150}$ for both ordered and disordered samples is shown in Fig. 12b. There is a positive and assymmetric deviation from linearity in $\Delta corr_{150}$ for the disordered (*C*2/*c*) solid solution, and its form is comparable to that of the enthalpy of mixing for this system (Wood *et al*., 1980). The difference in $\Delta corr_{150}$ between ordered (*P*2/*n*) and disordered (*C*2/*c*) samples, $\delta\Delta corr_{150}$, which relates to the difference in line width due to ordering, scales linearly with Q^2_{M1} (Fig. 12c), where Q_{M1} is the macroscopic order parameter derived from determinations of the cation populations of M1 sites.

The existence of line broadening in IR absorption spectra from samples with intermediate compositions across a solid solution implies that the crystals are locally heterogeneous. If there are structural heterogeneities, there must be strain gradients and, therefore, contributions to the excess enthalpy. It seems likely that autocorrelation analysis from crystals belonging to a solid solution series will, therefore, give insights into the enthalpy of mixing. An advantage of the spectroscopic approach is the fact that the resulting data appear to be much more precise, in relation to the total deviations from linearity, than data obtained by conventional calorimetry.

Acknowledgements: Support from the Natural Environment Research Council to MAC (grant no. GR3/10917) and from a European Union TMR network on Mineral Transformations (contract no. ERB-FMRX-CT97-0108) is gratefully acknowledged. Hinrich Meyer is thanked for his comments on the manuscript.

References

Atkinson, A.J., Carpenter, M.A., Salje, E.K.H. (1999): Hard mode infrared spectroscopy of plagioclase feldspars. *Eur. J. Mineral*., **11**, 7–21.

Boffa Ballaran, T., Carpenter, M.A., Domeneghetti, M.C., Salje, E.K.H., Tazzoli, V. (1998a): Structural mechanisms of solid solution and cation ordering in augite-jadeite pyroxenes: II. A microscopic perspective. *Am. Mineral*., **83**, 434–443.

—, —, —, —, — (1998b): Structural mechanisms of solid solution and cation ordering in augite-jadeite pyroxenes: I. A macroscopic perspective. *Am. Mineral*., **83**, 419–433.

Cellai, D., Carpenter, M.A., Wruck, B., Salje, E.K.H. (1994): Characterization of high-temperature phase transitions in single crystals of Steinbach tridymite. *Am. Mineral*., **79**, 606–614.

Cellai, D., Carpenter, M.A., Kirkpatrick, R.J., Salje, E.K.H., Zhang, M. (1995): Thermally induced phase transitions in tridymite: an infrared spectroscopic study. *Phys. Chem. Minerals*, **22**, 50–60.

Daniels, P., Wunder, B., Sahl, K., Schreyer, W. (1994): Changing lattice metrics of synthetic cordierites: the metastable hexagonal to orthorhombic transformation sequence during isothermal annealing. *Eur. J. Mineral*., **6**, 323–335.

de Dombal, R.F. & Carpenter, M.A. (1993): High-temperature phase transitions in Steinbach tridymite. *Eur. J. Mineral*., **5**, 606–622.

Dowty, E. (1987): Vibrational interactions of tetrahedra in silicate glasses and crystals: II. Calculations on melilites, pyroxenes, silica polymorphs and feldspars. *Phys. Chem. Minerals*., **14**, 122–138.

Görlich, E., Blaszczak, K., Handke, M. (1983): Infrared spectra of silica polymorphs. *Mineral. Polonica*, **14**, 3–18.

Graetsch, H. (1998): Characterization of the high-temperature modifications of incommensurate tridymite L3-T_o (MX-1) from 25 to 250°C. *Am. Mineral*., **83**, 872–880.

Güttler, B., Salje, E.K.H., Putnis, A. (1989): Structural states of Mg cordierite III: infrared spectroscopy and the nature of the hexagonal-modulated transition. *Phys. Chem. Minerals*., **16**, 365–373.

Hoffmann, W., Kockmeyer, M., Löns, J., Vach, Chr. (1983): The transformation of monoclinic low-tridymite to a phase with an incommensurate superstructure. *Fortschr. Miner*., **61**, 96–98.

Hofmeister, A.M., Rose, T.P., Hoering, T.C., Kushiro, I. (1992): Infrared spectroscopy of natural, synthetic and ^{18}O subsituted α-tridymite: structural implications. *J. Phys. Chem*., **96**, 10213–10218.

Kihara, K. (1978): Thermal change in unit-cell dimensions, and a hexagonal structure of tridymite. *Z. Krist*., **148**, 237–253.

Kihara, K., Matsumoto, T., Imamura, M. (1986): High-order thermal motion tensor analyses of tridymite. *Z. Krist*., **177**, 39–52.

Kitchin, S.J., Kohn, S.C., Dupree, R., Henderson, C.M.B., Kihara, K. (1996): *In situ* ^{29}Si MAS NMR

studies of structural phase transitions of tridymite. *Am. Mineral*., **81**, 550–560.

Landau, L.D. & Lifshitz, E.M. (1980): Statistical physics, 3rd edition, part 1. Pergamon Press, Oxford, 544 p.

Malcherek, T., Kroll, H., Schleiter, M., Salje, E.K.H. (1995): The kinetics of the monoclinic to monoclinic phase transition in $BaAl_2Ge_2O_8$-feldspar. *Phase Trans*., **55**, 199–215.

Malcherek, T., Carpenter, M.A., Kroll, H., Salje, E.K.H. (1999): Cation ordering in $B\underline{a}Al_2Ge_2O_8$-feldspar: implications for the $I\bar{1} \leftrightarrow C\bar{1}$ phase transition in anorthite. *Phys. Chem. Minerals*, **26**, 354–366.

Petzelt, J. & Dvorjak, V. (1984): Infrared spectroscopy of structural phase transitions in crystals. *in* "Vibrational spectroscopy of phase transitions", Z. Iqbal & F.J. Owens, eds., Academic Press, Orlando, Florida, 56–144.

Press, W.H., Teulosky, S.A., Vetterling, W.T., Flannery, B.P. (1992): Numerical recipes in FORTRAN. Cambridge University Press, Cambridge, 492 p.

Putnis, A. (1980a): The distortion index in anhydrous Mg-cordierite. *Contrib. Mineral. Petrol*., **74**, 135–141.

— (1980b): Order-modulated structures and the thermodynamics of cordierite reactions. *Nature*, **287**, 128–131.

Putnis, A. & Bish, D.L. (1983): The mechanism and kinetics of Al, Si ordering in Mg-cordierite. *Am. Mineral*., **68**, 60–65.

Putnis, A. & Angel, R.J. (1985): Al, Si ordering in cordierite using "magic angle spinning" NMR. II. Models of Al, Si order from NMR data. *Phys. Chem. Minerals*, **12**, 217–222.

Putnis, A., Salje, E., Redfern, S.A.T., Fyfe, C.A., Strobl, H. (1987): Structural states of Mg-cordierite I: order parameters from synchrotron X-ray and NMR data. *Phys. Chem. Minerals*, **17**, 446–454.

Redfern, S.A.T., Salje, E., Maresch, W., Schreyer, W. (1989): X-ray powder-diffraction and infrared study of the hexagonal to orthorhombic phase transition in K-bearing cordierite. *Am. Mineral*., **74**, 1293–1299.

Salje, E.K.H. (1992): Hard mode spectroscopy: experimental studies of structural phase transitions. *Phase Trans*., **37**, 83–110.

— (1994): Phase transitions and vibrational spectroscopy in feldspars. *in* "Feldspars and their Reactions", I..Parsons, ed. *NATO ASI Series C*, **421**, 103–160.

Salje, E.K.H. & Bismayer, U. (1997): Hard mode spectroscopy: the concept and applications. *Phase Trans*., **63**, 1–75.

Withers, R.L., Thompson, J.G., Xiao, Y., Kirkpatrick, R.J. (1994): An electron diffraction study of the polymorphs of SiO_2 tridymite. *Phys. Chem. Minerals*, **21**, 421–433.

Wood, B.J., Holland, T.J.B., Newton, R.C., Kleppa, O.J. (1980): Thermochemistry of jadeite-diopside pyroxenes. *Geochim. Cosmochim. Acta*, **44**, 1363–1371.

Yagil, Y., Baudenbacher, F., Zhang, M., Birch, J.R., Kinder, H., Salje, E.K.H. (1995): Optical properties of $YBa_2Cu_3O_{7-\delta}$ thin films. *Phys. Rev. B*, **52**, 1–9.

Xiao, Y., Kirkpatrick, R.J., Kim, Y.J. (1993): Structural phase transitions of tridymite: a ^{29}Si MAS NMR investigation. *Am. Mineral*., **78**, 241–244.

—, —, — (1995): Investigations of MX-1 tridymite by ^{29}Si MAS NMR - modulated structures and structural phase transitions. *Phys. Chem. Minerals*, **22**, 30–40.

Received 31 May 1999
Modified version received 26 January 2000
Accepted 27 January 2000